

Short-distance production of three particles with large scattering length

T. G. Backert^{1,*}, S. Dietz^{1,†}, H.-W. Hammer^{1,2,‡}, S. König^{3,1,§} and D. T. Son^{4,¶}

¹Technische Universität Darmstadt, Department of Physics, 64289 Darmstadt, Germany
²ExtreMe Matter Institute EMMI and Helmholtz Forschungssakademie Hessen für FAIR (HFHF), GSI Helmholtzzentrum für Schwerionenforschung GmbH, 64291 Darmstadt, Germany

³Department of Physics and Astronomy, North Carolina State University, Raleigh, NC 27695, USA
⁴Leinweber Institute for Theoretical Physics, University of Chicago, Chicago, IL 60637, USA

(Dated: January 28, 2026)

The short-distance production of multi-particle states in high-energy nuclear reactions provides a unique way to study the low-energy properties of few-body systems. In particular, the production amplitude of multi-neutron systems is strongly constrained by an approximate conformal symmetry of the underlying theory. We calculate the full amplitude for the short-distance production of three particles with large scattering length in leading order pionless EFT, focusing on the cases of three neutrons and three spinless bosons. We investigate the signature of low-energy resonances and other correlations in the relative energy distributions. For the case of neutrons, we compare to the predictions from approximate conformal symmetry close to the unitary limit and calculate the range corrections up to next-to-next-to-leading order.

I. INTRODUCTION

Short-distance particle production provides a powerful tool for probing the interactions of the produced particles. At ALICE, for example, the femtoscopy method is used to extract low-energy scattering parameters from the correlation functions measured in heavy ion collisions [1]. In this paper, we investigate the short-distance production of multi-particle states, focusing on the cases of three neutrons and three spinless bosons. The short-distance production of neutrons can be realized experimentally in high-energy nuclear reactions, assuming factorization of the production cross section [2, 3]. Such reactions provide a method to study multi-neutron systems [4].

The study of multi-neutron systems has a long and venerable history [5, 6]. In addition to their fundamental importance in nuclear physics, multi-neutron systems also provide a window on nuclear many-body forces with extreme isospin. This topic has received renewed interest with several experiments looking for tetraneutron clusters. Marqués and collaborators observed six events that exhibit the characteristics of a multi-neutron cluster liberated in the proton-induced breakup of ^{14}Be by detecting the recoiling proton [7]. Subsequently, a few events pointing towards a $4n$ resonance were measured in the reaction $^4\text{He}(^8\text{He}, ^8\text{Be})4n$ [8]. Another experiment using the reaction $^7\text{Li}(^7\text{Li}, ^{10}\text{C})$ even suggested that the tetraneutron could be bound [9]. The most convincing evidence for a resonance-like structure to date with much higher statistics, however, was recently presented by Duer *et al.* in an experiment using the reaction

$^8\text{He}(p, p\alpha)4n$ [4]. Whether the resonance-like structure seen in the experiment of Ref. [4] is a genuine resonance or due to some other effect, such as the final state interaction among dineutrons and/or the presence of pre-existing four-neutron correlations from the ^8He nucleus projectile [10] remains an open question. A non-standard hypothesis that is able to reconcile all experimental findings was proposed in Ref. [11]. The central observable in hard knock-out reactions, such as $^8\text{He}(p, p\alpha)4n$, is the relative energy (or center-of-mass energy) distribution of the neutrons, i.e., the energy distribution in the reference frame moving with the center-of-mass of the neutrons. In such a high-energy reaction, the neutrons are created in a very small spatial region in the order of 2.5 fm – roughly the size of ^8He [12, 13]. Typically, most of the kinetic energy transferred to the neutrons in the hard knock-out reaction is carried by the motion of their center of mass. This ensures that the dominant final state interaction after the knock-out is only among the neutrons, which have a low relative energy.

In this paper, we investigate the qualitative properties of such a multi-neutron state created at short distances in pionless EFT [14–17]. We focus on the production of three neutrons in a point and leave the extension to four neutrons and the effects of an extended source distribution for future work. Similar calculations for the case of three neutral charm mesons can be found in Refs. [18, 19]. The point-production is calculated applying effective potentials derived from pionless effective field theory (EFT) at leading order (LO) (see Ref. [20] for details) and next-to-next-to-leading order (N^2LO).

A particular focus is placed on the explicit verification of the constraints from non-relativistic conformal symmetry on the energy distribution of the neutrons [3]. For relative energies E in the range $1/(ma^2) \approx 0.1 \text{ MeV} \ll E \ll 1/(mr^2) \approx 5 \text{ MeV}$, where a and r are the scattering length and effective range of the neutrons, respectively, the system is effectively scale invariant. This universal regime is known as the unitary (or unitarity) limit

* timothy-george.backert@tu-darmstadt.de

† sebastian.dietz@physik.tu-darmstadt.de

‡ hans-werner.hammer@physik.tu-darmstadt.de

§ skoenig@ncsu.edu

¶ dtson@uchicago.edu

and plays an important role in many strongly interacting systems ranging from ultracold atoms to hadrons and nuclei [21–24]. In this regime the energy distribution is governed by power laws with exponents determined by the scaling dimensions of certain operators in the non-relativistic conformal field theory for the unitary limit. In addition, there is a second scale invariant region for very small energies, $E \ll 1/(ma^2)$, where the exponents are given by the scaling dimensions of the non-interacting theory. In this region, the energy spectrum simply follows the pure phase-space behavior. Both regions are connected to renormalization group fixed points of the coupling constant that determines the strength of the two-body contact interaction between neutrons [16]. Pionless EFT describes the full energy spectrum up to $E \lesssim 1/(mr^2)$ including the transition between the two scale-invariant regions. A related study focusing on the observability of the conformal exponents was presented in Ref. [25].

For comparison, we also consider the point-production of three spinless bosons, where genuine three-body resonances, are known to exist [20, 26–29]. In the negative scattering region, the Efimov bound states turn into resonances as they cross the three-body threshold as the scattering length is decreased. Thus they can be viewed as precursors to Efimov states. In this case, the continuous scale symmetry is broken down to a subgroup of discrete scaling transformations for three or more particles. As a consequence, physical observables show discrete scale invariance and Efimov physics [21, 30].

This paper is organized as follows. In Sec. II, we introduce the formalism required to calculate the point-production amplitude in pionless EFT. Our results are presented and discussed in Sec. III. In Sec. IV, we compare our results against existing theoretical and experimental results. The conclusion and an outlook are given in Sec. V. Since the corresponding integral equations are very similar, the three-neutron and three-boson cases are treated together unless noted otherwise.

II. POINT-PRODUCTION AMPLITUDE

Our aim is to calculate the relative energy distribution of the final state particles (neutrons or bosons), $R(E)$, up to a normalization factor that is regarded as arbitrary in this work. The distribution can be obtained by solving Faddeev equations for the point-production amplitude. For this, we follow the strategy of Refs. [31, 32] and use pionless EFT to construct an effective interaction potential as a sum of n -body potentials,

$$V_{\text{eff}} = \sum_{n=2}^{\infty} V_n. \quad (1)$$

In general, interaction terms up to $n = N$ contribute in a N -body problem, but at low energies higher-body terms are typically suppressed (this is described naturally

by dimensional analysis in the EFT, along with certain well-known exceptions; see, e.g., Ref. [24] for a review). The potentials V_n are constrained by Galilean symmetry and can be expressed in a momentum expansion. For S -wave two-body interactions, we have

$$\langle \mathbf{k}' | V_2 | \mathbf{k} \rangle = C_0 + C_2(\mathbf{k}'^2 + \mathbf{k}^2)/2 + \dots, \quad (2)$$

where \mathbf{k} and \mathbf{k}' are the relative momenta in the initial and final state. Regulator functions and spin-projection operators have been suppressed. Similar expansions can be written down for three- and higher-body interactions. In a multi-neutron system, only the momentum-independent two-body contact interaction C_0 in the 1S_0 channel contributes at leading order in pionless EFT [33, 34]. In the three-boson system, in contrast, both a momentum-independent two-body and three-body contact interaction have to be included to properly renormalize the system [35, 36]. Assuming typical momenta of order $1/a$, the uncertainty of a leading-order pionless EFT calculation can be estimated as $|r/a|$, where r is the effective range and a the scattering length. For the three-neutron system with $a \approx -18.9$ fm and $r \approx 2.83$ fm [37–39], this leads to a theoretical uncertainty in the order of 15% at leading order – see Section A. The exact form of the effective potential, of course, depends on the specific regularization scheme used. However, low-energy observables are independent of the regularization scheme (up to higher-order corrections), and one can choose any convenient scheme for practical calculations. In this work, we consider two different schemes, a soft Gaussian regulator and a sharp cutoff on momentum loop integrals.

The point-production amplitude $\Gamma_l(E; p)$ is obtained from the Faddeev equation for the particle-dimer amplitude shown in Fig. 1,

$$\Gamma(E; \mathbf{p}) = \sum_l (2l + 1) \Gamma_l(E; p) P_l(\cos \theta_p), \quad (3)$$

by projecting on the partial wave l . It applies to the three-boson and three-neutron systems simultaneously. The unified treatment is possible since the running three-body force in the three-boson system vanishes at a discrete set of ultraviolet cutoffs Λ due to its limit-cycle behavior. Thus one may choose to work with a specific cutoff $\Lambda = \Lambda_0$ in Eq. (4) where the explicit three-body term in the Faddeev equation vanishes [40]. We emphasize that this is merely a choice for technical convenience and that the physics of the three-body force is fully incorporated through the specific value of the cutoff Λ_0 . In the three-neutron case, there is no leading-order three-neutron force due to Fermi statistics disallowing such an interaction. Here, the solution is not sensitive to the cutoff Λ as long as Λ is sufficiently large.

Apart from the cutoff, both Faddeev equations only differ by a spin-isospin factor λ , which takes the values $\lambda = 1$ for the three-boson and $\lambda = -1/2$ for the three-neutron system, respectively.

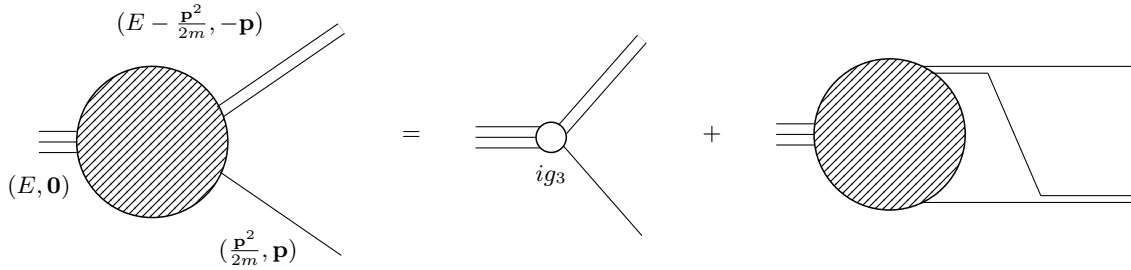


Figure 1. Integral equation for the point-production amplitude of a particle-dimer system with total energy E and total momentum $\mathbf{P} = 0$. Single (double) lines denote particles (dimers), while g_3 is the strength of the point source that creates the particle-dimer pair.

The equation for the partial wave projected production amplitude $\Gamma_l(E; p)$ reads

$$\Gamma_l(E; p) = g_{3,l} p^{l+2\delta_{l0}\delta_{2\lambda,-1}} + \lambda \frac{2}{\pi} \int_0^\Lambda dq q^2 Z_{2,l}(E; q, p) \tau(E; q) \Gamma_l(E; q), \quad (4)$$

where

$$\tau(E; q) = \left[-\frac{1}{a} + \sqrt{mE_q} \right]^{-1} \quad \text{with} \quad mE_q \equiv \frac{3}{4}q^2 - mE - i\varepsilon, \quad (5)$$

and

$$Z_{2,l}(E; q, p) = \int_{-1}^1 dx \frac{P_l(x)}{p^2 + q^2 + pqx - mE - i\varepsilon}. \quad (6)$$

$Z_{2,l}$ and τ are the two-body interaction kernel and the dimer propagator, respectively, and the limit $\varepsilon \rightarrow 0^+$ is understood at the end of the calculation. Notice, that for the three-fermion system the S -wave source contains a factor p^2 due to Pauli statistics (see Table II). Equation (4) describes the amplitude for the point creation of a dimer with two-body scattering length a and a single particle with angular momentum l (relative to the dimer), where $g_{3,l}$ is the strength of the point source. In the following, this strength will be set to unity for convenience. Together with further factors appearing later in the derivation, the source strength can be understood as a parameter of the theory that determines the overall normalization and has to be fitted to (experimental) data. The treatment of effective range corrections in the three-neutron case is discussed in Appendix A.

From the particle-dimer amplitude Γ_l , the full three-body amplitude $\bar{\Gamma}_l$ can be calculated by attaching an external dimer propagator and a coupling vertex for the break-up into two particles. Here, a difference between the bosonic and fermionic systems arises because of the different statistics. While $\bar{\Gamma}_l$ for the three-boson system is given by the symmetrized sum of all possible permutations of the outgoing particles, the anti-symmetrized sum of the permutations of identical fermions must be used for the three-neutron system.

A. Three bosons

First, we consider the three-boson system, using a soft Gaussian cutoff¹. In general, for three distinguishable particles, there are $3! = 6$ permutations. However, three of the six permutations are equivalent to the remaining ones, such that only three terms have to be considered. The amplitude is depicted in Fig. 2, where it is implicitly assumed that all outgoing particle lines are on-shell. The corresponding equation for the amplitude $\bar{\Gamma}_l$ reads:

$$\begin{aligned} \bar{\Gamma}_l(E; \mathbf{p}, \mathbf{k}) &= \Gamma_l(E; \mathbf{p}) \tau(E; -\mathbf{p}) P_l(\cos \theta_{\mathbf{p}, \mathbf{k}}) \\ &+ \left(\mathbf{p} \leftrightarrow -\frac{\mathbf{p}}{2} + \mathbf{k} \right) + \left(\mathbf{p} \leftrightarrow -\frac{\mathbf{p}}{2} - \mathbf{k} \right) \end{aligned} \quad (7)$$

$$\bar{\Gamma}(E; \mathbf{p}, \mathbf{k}) := \sum_l (2l+1) \bar{\Gamma}_l(E; \mathbf{p}, \mathbf{k}).$$

where Γ_l is calculated using Eq. (4) with $\lambda = 1$. We note that our definition of the partial-wave projected amplitude $\bar{\Gamma}_l$, directly includes the Legendre polynomial that describes the angular dependence. Finally, the symmetrized amplitude can be used to calculate the point-

¹ Explicit forms for the effective potentials and more detailed discussions are given in Ref. [20].

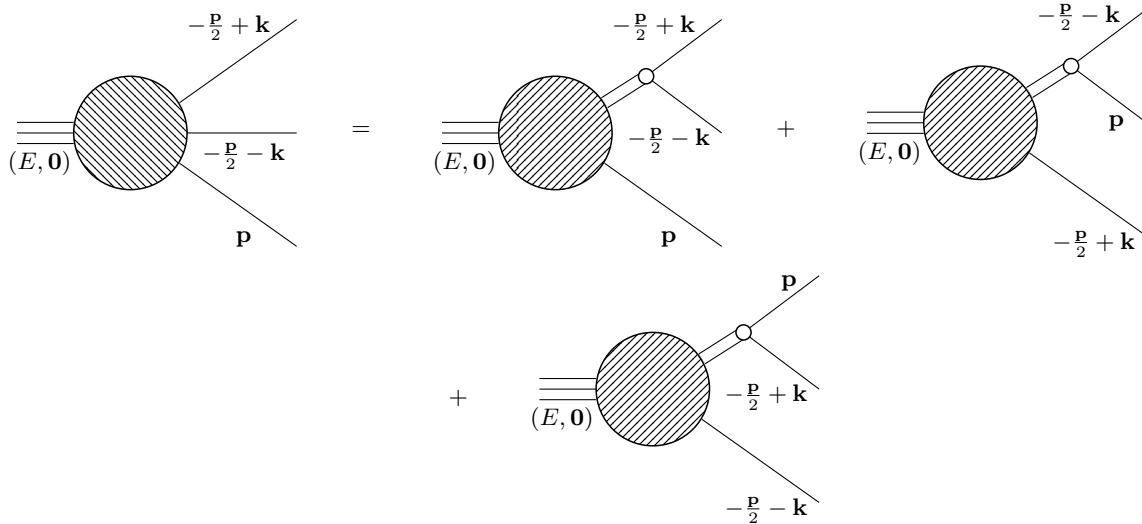


Figure 2. Fully symmetrized point-production amplitude $\bar{\Gamma}_l$ for three bosons. The bosons are produced with total energy E in their center-of-mass, such that the total momentum is $\mathbf{P} = 0$. The outgoing bosons are on-shell with the momenta given in the figure.

production energy distribution $R(E)$. It is defined as the phase-space integral of $|\bar{\Gamma}(E; \mathbf{p}, \mathbf{k})|^2$,

$$R(E) = \iint \frac{d^3 k d^3 p}{(2\pi)^6} |\bar{\Gamma}|^2 2\pi \delta [E - E_{\text{on-shell}}], \quad (8)$$

where the δ -function ensures the energy conservation of the three outgoing on-shell bosons with energy $E_{\text{on-shell}} = E_{\mathbf{p}} + E_{-\frac{\mathbf{p}}{2} + \mathbf{k}} + E_{-\frac{\mathbf{p}}{2} - \mathbf{k}}$. The energy conserving δ -function can be simplified by applying the variable transformation for δ -distributions, which results in

$$\begin{aligned} \delta [E - E_{\text{on-shell}}] &= \delta \left[E - \left(\frac{3p^2}{4m} + \frac{k^2}{m} \right) \right] \\ &= \frac{m}{2} \frac{\delta \left[k - \sqrt{mE - \frac{3}{4}p^2} \right]}{\sqrt{mE - \frac{3}{4}p^2}}. \end{aligned} \quad (9)$$

Note that the argument of the square root cannot become negative since energy conservation limits the value of $p \leq \sqrt{\frac{4}{3}mE}$.

B. Three neutrons

Next, we consider a system of three neutrons. For this case, we show results obtained with a sharp-cutoff regulator.² According to the Pauli principle, the amplitude

now needs to be anti-symmetrized with respect to identical particles. The two neutrons emerging from the dimer have opposite spins, since identical fermions do not interact in the S -wave. Consequently, only two of the three final-state neutrons have the same spin orientation and the amplitude must be antisymmetric under exchange of these two neutrons. The corresponding anti-symmetrized amplitude Γ_l is shown diagrammatically in Fig. 3, where again all outgoing particle lines are on-shell.

The amplitude $\bar{\Gamma}_l$ can be written as

$$\begin{aligned} \bar{\Gamma}_l(E; \mathbf{p}, \mathbf{k}) &= \Gamma_l(E; \mathbf{p}) \tau_l(E; -\mathbf{p}) P_l(\cos \theta_{\mathbf{p}, \mathbf{k}}) \\ &\quad - \left(\mathbf{p} \leftrightarrow -\frac{\mathbf{p}}{2} + \mathbf{k} \right), \end{aligned} \quad (10)$$

where Γ_l is calculated using Eq. (4) with $\lambda = -1/2$.

As we did for three bosons, our aim is to calculate the point-production distribution $R(E)$ from this amplitude. It is defined analogously to Eq. (8), where the connection between $\bar{\Gamma}$ and $\bar{\Gamma}_l$ is given by Eq. (7). Here, we will consider partial waves up to the D -wave, demonstrating that P -wave is the dominant. We will look at the individual contributions of S , P , and D -waves, as well as their sum including all interference terms.

The full point-production distribution up to $l = 2$ is given by

$$\begin{aligned} R(E) &= \frac{m}{8\pi^3} \int_0^{\sqrt{4mE/3}} dp p^2 \sqrt{mE - \frac{3}{4}p^2} \\ &\quad \times \int_{-1}^{+1} d \cos \theta_{\mathbf{p}, \mathbf{k}} \left| \sum_{l=0}^2 (2l+1) \bar{\Gamma}_l(E; \mathbf{p}, \mathbf{k}) \right|^2, \end{aligned} \quad (11)$$

where $|\mathbf{k}| = k = \sqrt{mE - \frac{3}{4}p^2}$ due to the delta distribution in the integral. To obtain the contribution of indi-

² Indeed, we performed the three-neutron calculations using both a soft Gaussian regulator and a sharp cutoff, obtaining consistent results. In the text, we show the sharp-cutoff results.

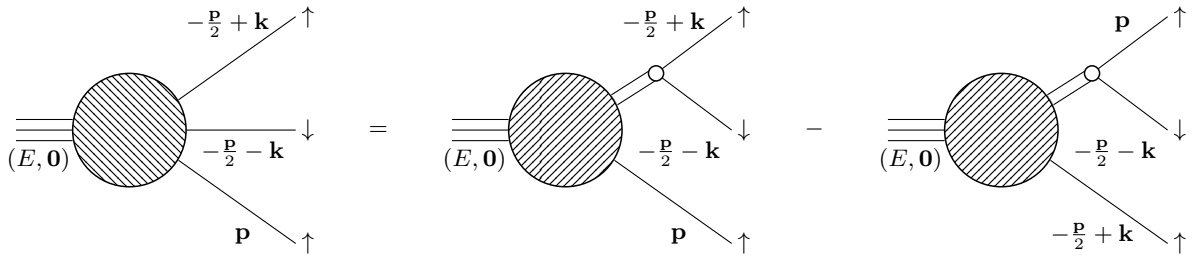


Figure 3. Anti-symmetrized point-production amplitude $\bar{\Gamma}_l$ for three neutrons. The neutrons are produced with total energy E in their center-of-mass, such that the total momentum is $\mathbf{P} = 0$. The outgoing neutrons are on-shell with the momenta and spins indicated in the figure.

vidual partial waves, we set the contribution of the other partial waves to zero. In this case there are no interference terms, by construction.

III. RESULTS

We are now in the position to calculate the point-production amplitudes and study their behavior.

A. Three bosons

We start with the three-boson case, for which we set the boson mass equal to the neutron mass, to make it easy to compare to the three-neutron results (discussed below). Efimov states for negative scattering length a are known to evolve into resonances as they cross the three-particle threshold [20, 26–29]. Thus, it is interesting to investigate the signature of the resonances in the point-production amplitude. To calculate the point-production distribution, we solve the integral equation (4) for Γ_l . Here, we use effective potentials with a smooth Gaussian cutoff. For details, see Ref. [20]. We focus on the case where the third boson is in a relative S -wave, $l = 0$, which is the dominant contribution at low energies. As discussed above, we choose a renormalization scheme where the three-body force is set to zero and the three-body parameter is varied by changing the cutoff Λ in Eq. (4). The integral equation features a three-body branch cut along the positive real energy axis. To deal with this, we calculate Γ_0 not on the real axis, but slightly shifted onto the first quadrant of the complex energy plane, $E \rightarrow E + i\varepsilon$. In the end, one has to extrapolate to $\varepsilon = 0$, or at least choose $\varepsilon \ll \text{Re}\{E\}$. Figure 4 shows the resulting point-production distribution for different imaginary parts $\text{Im } E$ of the complex energy. In the limit $\varepsilon = \text{Im } E \rightarrow 0$, the physical result is obtained. The parameter values $\Lambda = 179.9 \text{ fm}^{-1}$ and $a = -12.6 \text{ fm}$ and were chosen such that $a_-/a = 1.5$, where a_- is the scattering length at which the pole trajectory crosses the three-body branch cut. The curves for the two smallest values of $\text{Im } E$ are indistinguishable and show a peak

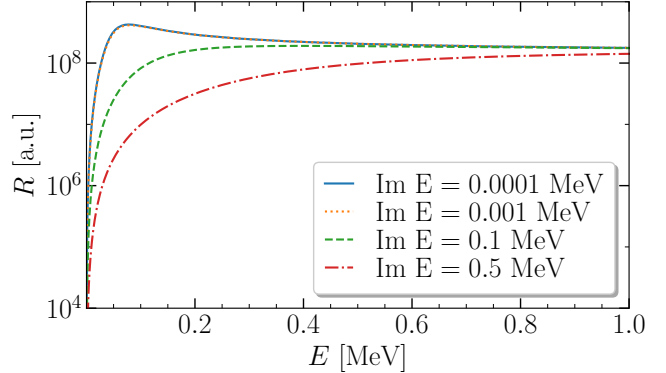


Figure 4. The point-production distribution for the three-boson system with $\Lambda = 179.9 \text{ fm}^{-1}$ and $a = -12.6 \text{ fm}$, corresponding to $a_-/a = 1.5$, for different values of the artificial imaginary part of the energy E . The curves for the two smallest values are indistinguishable. In the limit $\text{Im } E \rightarrow 0$ the physical amplitude is obtained.

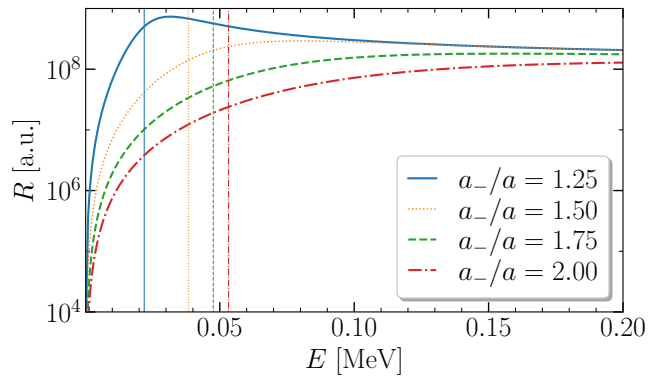


Figure 5. The physical point-production distribution in the limit $\text{Im } E \rightarrow 0$ for different ratios of a_-/a . The parameter values are $\Lambda = 179.9 \text{ fm}^{-1}$ and $a = -15.12, -12.6, -10.8$, and -9.45 fm .

close to threshold. In order to investigate the connection of the peak position to real part of the resonance energy, we show in Fig. 5 the point-production distribution

calculated for different values of a_-/a . In practice, this was done by keeping $\Lambda = 179.9 \text{ fm}^{-1}$ fixed and taking the scattering length as $a = -15.12, -12.6, -10.8$, and -9.45 fm . In Fig. 5, we show the results for the physical point-production distribution for $a_-/a = 1.25, 1.5, 1.75$, and 2.0 . The real part of the Efimov resonance energy calculated from an analytical continuation [20] is indicated by a vertical line.

The resonance energies and widths from the analytical continuation are also collected in Tab. I. For small widths Γ , the peak position of the point-production distribution gives a good estimate of the real part of the resonance energy. However, for larger resonance widths the difference between the two positions becomes larger and ultimately the peak disappears altogether. At $a = -18.9 \text{ fm}$, $a_-/a = 1$ and the resonance turns into an Efimov state directly at the three-body threshold, which becomes bound when $|a|$ is increased even further. Our calcula-

a_-/a	$E \text{ [MeV]}$	$\Gamma/2 \text{ [MeV]}$
1.10	0.010	0.003
1.25	0.022	0.014
1.50	0.037	0.040
1.75	0.048	0.074
2.00	0.053	0.113

Table I. The resonance energies and widths for different scattering length calculated using the analytical continuation [20]. The transition to a bound state takes place at $a_- = -18.9 \text{ fm}$.

tions agree with earlier calculations of near-threshold Efimov resonances in the three-boson system via transition operators on the real energy axis in Ref. [27]. Moreover, they demonstrate that the point-production distribution contains information about near-threshold resonances and therefore serve as a benchmark for our investigation of the three-neutron system.

B. Three neutrons

While the three-boson system at LO is determined by two scales, the scattering length a and the three-body force (or equivalently the cutoff Λ), the three-neutron system features only one scale at leading order, the scattering length a . In the unitary limit of infinite scattering length, the system exhibits an extended symmetry, the so-called Schrödinger or non-relativistic conformal symmetry. Thus the system can be considered as an approximate realization of an “unparticle” or “unnucleus” [3].

A multi-neutron system can be described approximately by a field in a non-relativistic conformal field theory that is characterized by two parameters, a scaling dimension Δ and its mass M [41]. The approximate conformal description is applicable to multi-neutron systems

with center-of-mass energies in the range

$$\frac{1}{ma^2} \approx 0.1 \text{ MeV} \ll E \ll \frac{1}{mr^2} \approx 5 \text{ MeV}, \quad (12)$$

where, in first approximation, the scales $1/(ma^2)$ and $1/(mr^2)$ can be taken to 0 and infinity, respectively. The region of energies $E \lesssim 1/(ma^2)$ can be calculated in standard pionless EFT, which includes the effects of finite a . Since we apply pionless EFT at LO in our numerical calculations of three-neutron systems, the effective range r effectively takes the value zero³. Therefore, our results show conformal behavior up to arbitrarily high energy, but this behavior is nonphysical for $E \gtrsim 1/(mr^2)$.

In the conformal region, the energy dependence of the point-production distribution R is solely determined by the scaling dimension of the conformal field (up to an overall normalization). Specifically, it scales as [3]

$$R(E) \sim E^{\Delta - \frac{5}{2}}, \quad (13)$$

where Δ is the scaling dimension of the conformal field representing the multi-neutron state.

For very small energies $E \ll 1/(ma^2)$, the system is described by the scaling dimensions of the non-interacting theory, which are determined by naive dimensional analysis. A free field is characterized by the scaling dimension $\Delta = 3/2$. Thus the energy dependence of the point-production amplitude for N particles is given by Eq. (13), with Δ replaced by

$$\Delta_{\text{free}} = \frac{3N}{2} + \#\nabla + 2 \times \#\partial_t, \quad (14)$$

where $\#\nabla$ and $\#\partial_t$ are the number of spatial or time derivatives included in the composite operator \mathcal{O} that represents the multi-neutron state. An overview of the field operators \mathcal{O} in terms neutron fields ψ_\downarrow and ψ_\uparrow with the lowest scaling dimensions Δ of multi-neutron systems up to six neutrons is given in Tab. II.

N	S	L	\mathcal{O}	Δ	Δ_{free}
2	0	0	$\psi_\uparrow \psi_\downarrow$	2	3
3	1/2	0	$\psi_\uparrow \psi_\downarrow \partial_t \psi_\uparrow$	4.66622	6.5
3	1/2	1	$\psi_\uparrow \psi_\downarrow (\nabla_i \psi_\uparrow)$	4.27272	5.5
3	1/2	2	$\psi_\uparrow \psi_\downarrow \nabla_i \nabla_j \psi_\uparrow$	5.60498	6.5
4	0	0	$\psi_\uparrow \psi_\downarrow (\nabla_i \psi_\uparrow) (\nabla_i \psi_\downarrow)$	5.028	8
5	1/2	1	$\psi_\uparrow \psi_\downarrow (\nabla_i \psi_\uparrow) (\nabla_i \psi_\downarrow) (\nabla_j \psi_\uparrow)$	7.53	10.5
6	0	0	$\psi_\uparrow \psi_\downarrow ((\nabla_i \psi_\uparrow) (\nabla_i \psi_\downarrow))^2$	8.48	13

Table II. An overview of the operators \mathcal{O} with the lowest scaling dimension for different particle numbers N in the vicinity of the strongly interacting and free fixed points [42]. S and L denote the corresponding spin and orbital angular momentum. Repeated indices are summed over.

³ That is, $r \rightarrow 0$ in the limit $\Lambda \rightarrow \infty$. Depending on the particular regularization scheme used to implement the EFT, at finite Λ , r may take values that are $\mathcal{O}(1/\Lambda)$, which can be neglected for sufficiently large Λ .

To begin with, one finds that the point-production distributions follow the predictions by conformal theory for the low and high energy range (details are given in Appendix B). However, the partial-wave point-production distributions for these three partial waves can also be compared with each other (cf. Fig. 6). Assuming the same strength of the source term $g_{3,l} = 1$ for all partial waves, the dominant contribution is due to the P -wave. Under this assumption, the full amplitude up to the D -

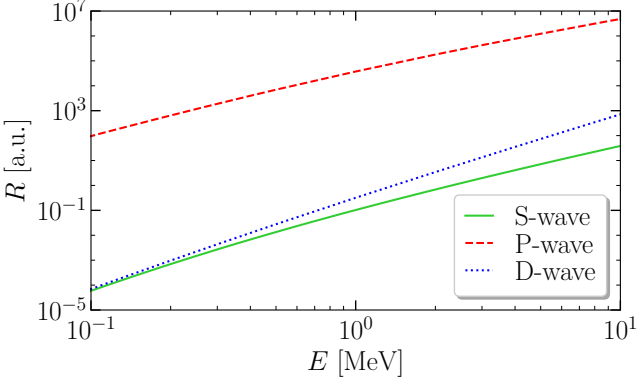


Figure 6. The partial-wave point-production distributions for the three partial waves considered. For all partial waves an equal strength of the source term, $g_{3,l} = 1$ is assumed.

wave is nearly the same in comparison to the P -wave amplitude, see Fig. 6. With this, the central result of this analysis is that, unlike in the three-boson system, the full three-neutron amplitude shows *no evidence of any resonance-like structure*. This is in line with previous studies [20, 43–45].

However, it is still interesting to study nearly conformal behavior in the three-neutron system, as discussed above. For each partial wave, we introduce a dimensionless function $\mathcal{R}(x)$ via

$$R(E) = c\mathcal{R}(x)E^{\Delta-5/2} \quad \text{for } x = Ema^2, \quad (15)$$

with the conformal scaling dimension Δ and some constant c such that $\mathcal{R}(x) \rightarrow 1$ for $x = Ema^2 \rightarrow \infty$. In this way, one can study how rapidly the conformal limit is reached within our pionless EFT. Investigating the approach of the partial waves towards their respective conformal limits in Fig. 7 shows the following: while the P - and D -wave distributions approach the conformal limit at about $x \simeq 100$, corresponding to about $E \simeq 10$ MeV, the S -wave distribution approaches the conformal limit much slower and only at higher energies. We further note that compared to P - and D -wave the S -wave converges more slowly, requiring a careful tuning of the artificial imaginary part of the energy ϵ from Eqs. (5) and (6) – for more details see Appendix B.

In Appendix A, we calculate the effective range corrections to the point-production distributions treating the effective range non-perturbatively [34, 46]. This amounts to a pionless EFT calculation that is accurate to N^2LO ,

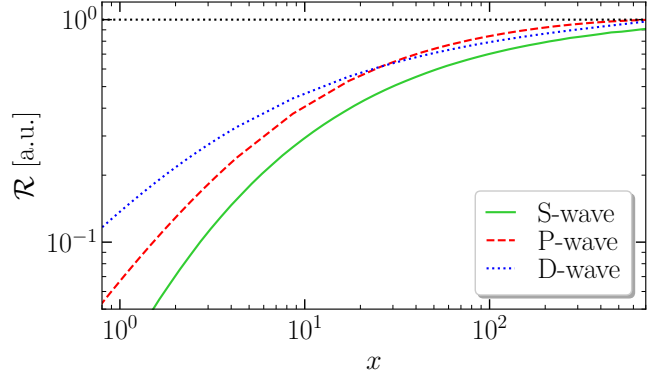


Figure 7. The partial wave point-production distributions for each partial wave considered in its universal form of $\mathcal{R}(x)$ with $x = Ema^2$, defined like in Eq. (15), such that $\mathcal{R}(x) \rightarrow 1$ for $x \rightarrow \infty$. The corresponding coefficients read $c \in [0.386, 9.91 \cdot 10^4, 0.723]$ (for S -, P -, D -wave).

but includes some higher-order range contributions. The range corrections turn out to be very small, consistent with the their perturbative evaluation in conformal field theory [47].

IV. COMPARISON WITH OTHERS

We can compare our results with the semi-classical Jeffries-Wentzel-Kramers-Brillouin (JWKB) approximation results of Higgins *et al.* [25]. Within their approach they extracted the effective power-law coefficient $\Delta_{\text{eff}} - 5/2$ from the relation $R \propto E^{\Delta_{\text{eff}}(E)-5/2}$. In other words, this is just the slope in the log-log plot shown in our Fig. 6. We performed the same kind of analysis for our pionless EFT data, shown in Fig. 8.

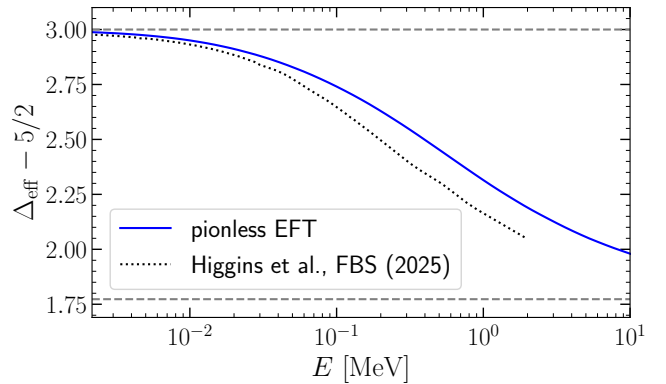


Figure 8. The effective power law coefficient for three neutron point production. Shown are the JWKB results (black dotted) from Higgins *et al.* [25] and our pionless EFT results (blue solid). For low or high energies the asymptotic values 3 or 1.773 predicted by conformal field theory (horizontal dashed lines).

In Ref. [25], the authors also plot the effective exponent for larger values of the scattering length. Compared to our pionless EFT calculation, their exponent for the physical neutron-neutron scattering length shifts more rapidly as a function of the energy between the asymptotic values predicted by conformal theory (see Fig. 8). Upon closer inspection, one observes that the results of Higgins *et al.* [25] for larger values of the scattering lengths overshoot the asymptotic value of 1.773 at energies around 1 MeV, suggesting that a similar overshooting may occur for the physical scattering length at larger energies as well (cf. Fig. 3 of [25]). The reason for this is presumably that their hyper-radial potential curve includes some higher-order contributions. This appears to be consistent with our findings including effective range corrections in Appendix A that indicate that the conformal limit is not reached before the effective range becomes relevant. In summary, we confirm that the conformal theory asymptotics are not fully reached within the energy range of interest for the three-neutron continuum.

We can furthermore compare our theory calculations with recent experimental results from Miki *et al.* [48]. These authors studied the low-momentum charge exchange ${}^3\text{H}(t, {}^3\text{He})3n$ reaction to investigate the three-neutron continuum at intermediate energies. In Fig. 9 we compare our predictions from pionless EFT and conformal field theory with the actual experimental data from Ref. [48] for momentum transfers $q_{\text{cm}} = 22, 40 MeV to the three-neutron system. For these low momentum transfers, the three-neutron system is left almost undisturbed in the reaction.$

Overall, we see both qualitative and quantitative agreement between pionless EFT, conformal theory, and the experimental results. The experimental data are not precise enough to differentiate with the conformal prediction and the pionless EFT calculation which includes the effect of the finite scattering length. Moreover, there is no evidence for a resonance-like structure in the three-neutron continuum in the data of [48]. This is in agreement with the pionless EFT and conformal theory results obtained here. The conformal theory also excludes a resonance-like structure in the low-energy four-neutron continuum in agreement with most other theoretical calculations [6, 10]. Most recently, Wu *et al.* [49] investigated the tetraneutron system on the lattice and also reported no indication of a resonance. For us, this motivates further studies focused on the origin of the structure observed in the tetraneutron experiment of Ref. [4].

V. SUMMARY AND OUTLOOK

We studied the short-range production of three particles characterized by a large scattering length using pionless EFT. We introduced a point-production amplitude, which we then solved employing the Faddeev formalism. Due to the formal similarity between both systems, we

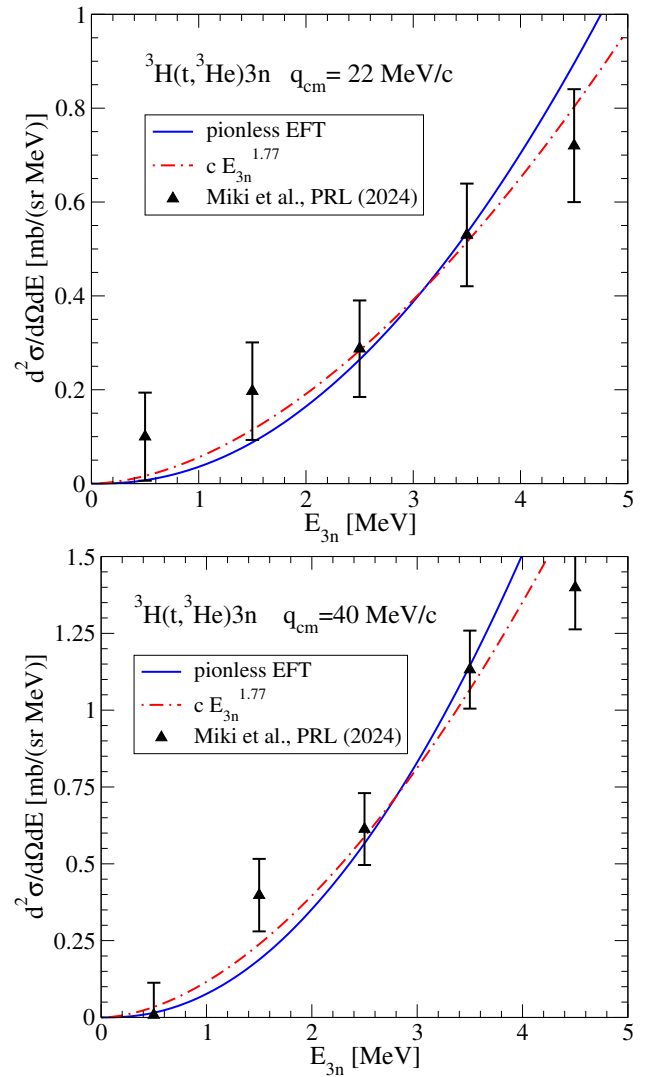


Figure 9. Differential cross section as a function of the relative energy between the three neutrons, illustrating the three-neutron continuum. Experimental results from Miki *et al.* [48] are compared with our theoretical results of pionless EFT and conformal field theory. The results are shown for average momentum transfer $q_{\text{cm}} = 22$ MeV/c (upper graph) and $q_{\text{cm}} = 40$ MeV/c (lower graph).

solved the Faddeev equations for both three identical bosons and three identical fermions, with particular focus on the potential appearance of resonance-like structures in the three-neutron system. In doing so, we compared our pionless EFT results with the findings of conformal field theory, which are valid in the unitary limit $1/a \rightarrow 0$ and $r \rightarrow 0$, corresponding to the high energy regime of pionless EFT at leading order. By analyzing each individual partial wave, we confirmed the presence of a resonance in the three-boson system, as expected from previous analyses [20, 26–29]. In contrast, no resonance-like structure was observed in the three-neutron system, again in line with previous studies [20, 43–45]. Upon examining S -, P - and D -waves for three neutrons, we

found that for natural values of the production strengths, $g_{3,l} \simeq 1$, the P -wave contribution is dominant. We also carried out a non-perturbative calculation of effective range corrections to the point-production distributions in Appendix A amounting to a pionless EFT calculation accurate to $N^2\text{LO}$. The range corrections are very small, consistent with the their perturbative evaluation in conformal field theory [47].

In light of recent and forthcoming tetraneutron experiments suggesting a structure in the final tetraneutron state [4], an analysis of the four-neutron system, similar to the one performed here for three neutrons, would be very interesting. In future work, we plan to do this using Faddeev-Yakubovsky formalism. From the perspective of conformal field theory, as discussed within this work, no such resonance structure is expected. This is in line with the findings of Ref. [10], who argue that the resonance-like structure reported in Ref. [4] is caused by the initial four-neutron configuration originating from the structure of ${}^8\text{He}$. Zhang *et al.* [50] recently found similar four-neutron configurations in nuclear Lattice EFT.

ACKNOWLEDGMENTS

This work was supported in part by the Deutsche Forschungsgemeinschaft (DFG, German Research Foundation) – Project ID 279384907 – SFB 1245 (T.G.B., S.D. and H.W.H.), by the BMFTR Contract No. 05P24RDB (H.W.H.), by the U.S. National Science Foundation under Grant No. PHY-2044632 (S.K.), and by the U.S. Department of Energy under Grant No. DE-FG02-13ER41958 (D.T.S.). This material is based upon work supported by the U.S. Department of Energy, Office of Science, Office of Nuclear Physics, under the FRIB Theory Alliance award DE-SC0013617 (S.K.). Computational resources for parts of this work were provided by the high-performance computing cluster operated by North Carolina State University, as well as by the Jülich Supercomputing Centre.

Appendix A: Effective range corrections

In this section, we incorporate the effective range $r = 2.83$ fm to obtain and analyze effective range corrections for both S - and P -wave.

To introduce the effective range in our theory, we adopt the two-body T-matrix from Eq. 5 as follows

$$\tau_{N^2\text{LO}}(E; q)^{-1} = \tau(E; q)^{-1} - \frac{r}{2} m E_q, \quad (\text{A1})$$

with $m E_q \equiv \frac{3}{4} q^2 - m E - i\varepsilon$.

By proceeding this way, which corresponds to a resummation of the terms associated with C_2 in Eq. (2), we include all contributions up to $N^2\text{LO}$ contributions and

even some of higher order [34, 46]. We note that in principle such corrections should be treated in perturbation theory, as dictated by the power counting. Moreover, in a calculation strictly based on a potential as in Eq. (2), one runs into the so-called “Wigner bound” that would limit the maximum value of our cutoff Λ [51–53]. However, in the diagrammatic formulation with dimer/dineutron fields, it is possible to avoid this bound (by implementing the range correction effectively as an energy-dependent potential). Since the resulting integral equation for three neutrons is well behaved [34, 46], we find it useful to use the resummed approach in order to estimate the influence of effective-range corrections. Their strictly perturbative treatment will be considered in future work. Aside from modifying the two-body T-matrix according to Eq. (A1), the procedure to determine the production distribution remains the same.

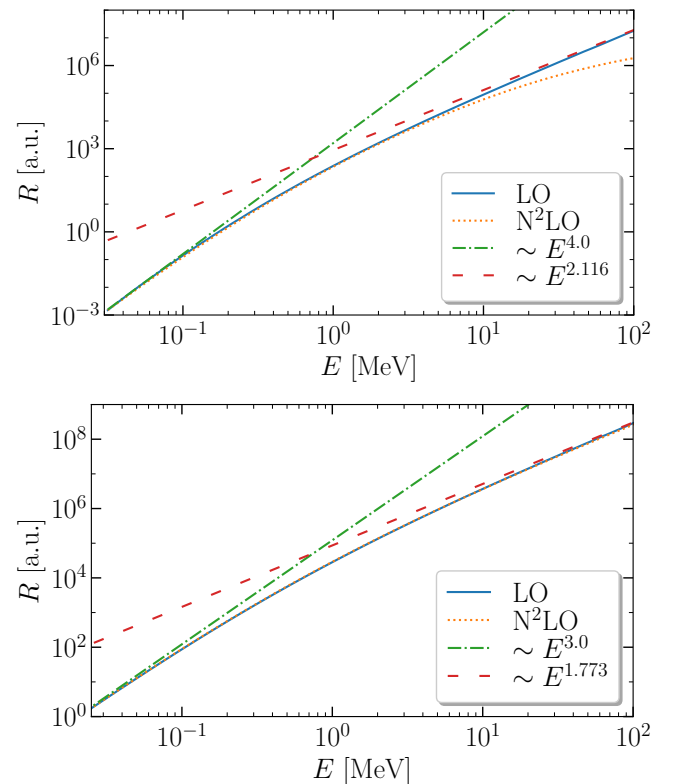


Figure 10. The partial-wave point-production distribution R for the three-neutron system for pionless EFT in LO (blue solid line) and $N^2\text{LO}$ (orange dotted line), with the third neutron in a relative S - and P -wave, are shown in the upper and lower panel, respectively. The small or high energy results can be compared to the predictions for free particles (green dash-dotted line) or non-relativistic conformal field theory (red loosely dashed line). We see very good agreement for both low and high energies at LO and $N^2\text{LO}$, with expected deviations at higher energies.

In Fig. 10 we plot S - and P -wave results in LO and $N^2\text{LO}$. The LO and $N^2\text{LO}$ results are consistent at low energies – as expected. However, as energy increases,

relative deviations emerge – at $1/(mr^2) \approx 5$ MeV about 20% for the S - and 0.4% for the P -wave, respectively. The S -wave is consistent with our rough estimate of $|r/a| \simeq 15\%$, but the effective range contribution to the P -wave is strongly suppressed. Notably, the effective range $r = 2.83$ fm plays a more significant role in the S -wave than in the P -wave results. This means up to $N^2\text{LO}$ the P -wave still reaches the conformal limit, while the S -wave does not – or only approximately so at about 10 MeV. However, these results are in line with the findings of Chowdhury *et al.* [47], which demonstrated that the first-order effective range correction to conformal theory vanishes exactly, making the effect of the effective range rather small. In fact, our numerical results are consistent with the subleading r^2 correction vanishing as well. Furthermore, the fact that the S -wave does not reach the conformal limit at $N^2\text{LO}$ is consistent with the

findings of Higgins *et al.* [25], but in their calculation the same was true for the P -wave as well, presumably since higher orders of the EFT expansion were effectively included.

Appendix B: Consistency with conformal predictions

In this section, we briefly discuss the less convergent nature of S -wave point-production, followed by a consistency check between conformal theory predictions and the low- and high-energy regime of our leading-order pionless EFT results.

Let us first consider the far off-shell limit $p^2 \gg E$ of Eq.(4) and apply a power-law ansatz for the point-production amplitude. This yields the following algebraic equation for the conformal scaling dimension of the S -wave channel [21]

$$\Gamma_0(E, p) \sim p^{\Delta-7/2} = p^2 - \frac{2}{\pi\sqrt{3}} p^{\Delta-7/2} \int_0^\infty dx x^{\Delta-7/2} \log \left[\frac{1+x+x^2}{1-x+x^2} \right]. \quad (\text{B1})$$

Taking closer look, using a sharp cutoff this integral scales as $\Lambda^{\Delta-7/2}$. Further, focusing on the asymptotic equation, which can be solved via identification as an (extended) Mellin transform. This leads to

$$1 = -\frac{4}{\sqrt{3}} \frac{\sin(s\pi/6)}{s \cos(s\pi/2)}, \text{ with } \Delta = s + 5/2. \quad (\text{B2})$$

One solution, we already expect from our conformal field theory findings, reads $\Delta = 4.66622$. However, for $\Delta = 4.66622$ the integral above does diverge like $\Lambda^{1.16622}$. In contrast, applying the same steps to higher partial waves yields an integral that is at least less divergent or even convergent. This owes to the presence of the angular-momentum potential barrier. One can easily verify this for the P - and D -wave. In these cases, the steps outlined above lead to an integral that scales like $\Lambda^{\Delta-9/2}$ or $\Lambda^{\Delta-11/2}$, respectively. For the conformal solutions $\Delta = 4.27272$ and $\Delta = 5.60498$, this corresponds to $\Lambda^{-0.22728}$ and $\Lambda^{0.10498}$, respectively. Based on this insight, we suggest that P - and D -wave calculations are “more convergent” than the S -wave one. However, it should be noted that we observed this behavior in the far off-shell regime. Taken together, we conclude that the diverging asymptotic solution of the S -wave integral-equation likewise signals the numerically observed instability, which occurs for S - but not the other partial waves. For our calculations, with $\text{Im}\{E\} = 10^{-4}$ MeV, shown in Eq. (11), this instability is evident for energies lower than $E \simeq 10^{-2}$ MeV. To extract the correct low-energy

behavior, the imaginary part of the energy ϵ must be tuned much more carefully and requires a much finer momentum mesh to achieve convergence than in the case of higher partial waves.

However, for fermion-dimer scattering the inhomogeneous term is not $\simeq p^2$ as in point-production, but instead suppressed like $\simeq p^{-2}$ at large momenta. As a consequence, each term of the perturbative Borne series converges, which is not the case for point-production. This again highlights the role of the special driving term in the point-production Faddeev equation. Moreover, comparing the bosonic case, with a driving term scaling as $\simeq p^0$, to the fermionic case, where it scales as $\simeq p^2$, we find – as expected – that the bosonic case exhibits better convergence.

In summary, we found differences in the convergence behavior of different partial waves in our point-production calculations, which can be traced back to the general structure of the three-body Faddeev equation, with particular emphasis on the role of the driving term.

Referring again to Fig. 11, we now compare our EFT results with the conformal predictions for the first partial waves, namely S , P and D -waves. For all three partial-wave channels the results for the point-production distribution agree reasonably well with these predictions. Of course this is as one would expect since the low energy regime $E \ll 1/(ma^2)$ corresponds to the free limit $a \rightarrow 0$ while the high energy regime $E \gg 1/(ma^2)$ corresponds to the unitary/conformal limit $|a| \rightarrow \infty$, noting that $r = 0$ fm within pionless EFT at leading order.

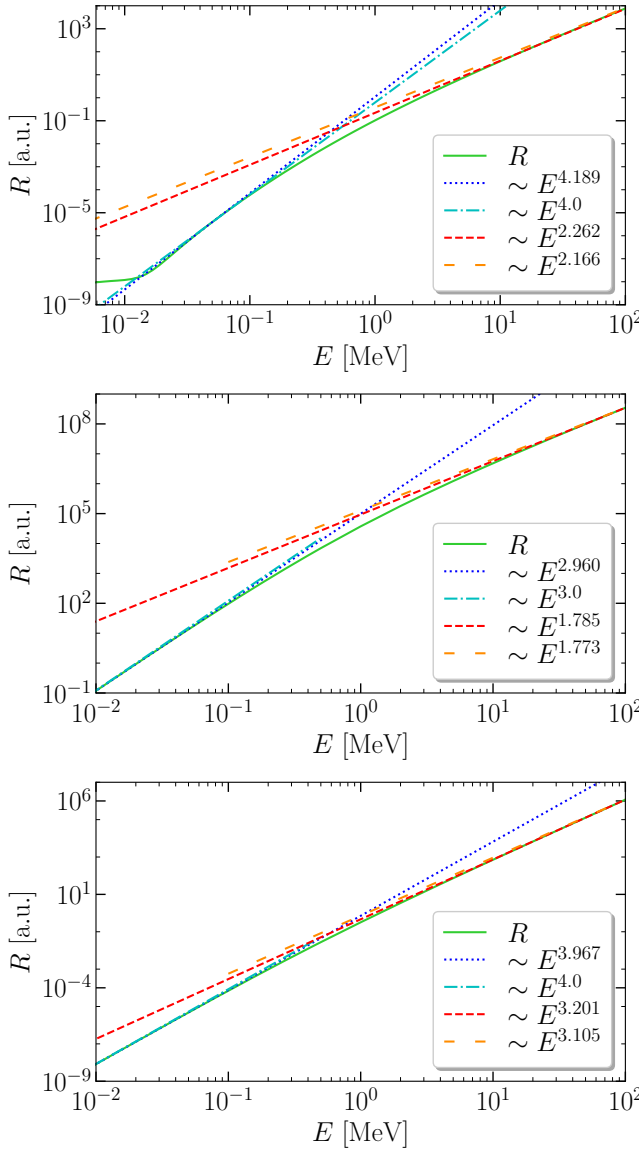


Figure 11. The partial-wave point-production distribution R for the three-neutron system, with the third neutron in a relative S -, P -, and D -wave, are shown in the upper, middle and lower panel, respectively. The results are fitted by a function $R(E) = aE^b$ at small ($E=0$ MeV, blue dotted line) as well as large energies ($E=100$ MeV, red dashed line). The small energy fit can be compared to the predictions for free particles (cyan dash-dotted line) as well as the fit at large energies to the predictions by non-relativistic conformal field theory (orange loosely dashed line). Both show a very good agreement between conformal theory and calculation.

[1] M. A. Janik (ALICE), Overview of recent femtoscopy measurements with ALICE, in *13th Workshop on Particle Correlations and Femtoscopy* (2018) arXiv:1811.02828 [hep-ex].
 [2] G. T. Bodwin, E. Braaten, and G. P. Lepage, Rigorous

QCD analysis of inclusive annihilation and production of heavy quarkonium, Phys. Rev. D **51**, 1125 (1995), [Erratum: Phys. Rev. D **55**, 5853 (1997)], arXiv:hep-ph/9407339.
 [3] H.-W. Hammer and D. T. Son, Unnuclear physics: Con-

formal symmetry in nuclear reactions, *Proc. Nat. Acad. Sci.* **118**, e2108716118 (2021), arXiv:2103.12610 [nucl-th].

[4] M. Duer *et al.*, Observation of a correlated free four-neutron system, *Nature* **606**, 678 (2022).

[5] R. Y. Kezerashvili, Search of trineutron and tetraneutron, in *6th International Conference on Fission and Properties of Neutron Rich Nuclei* (2016) arXiv:1608.00169 [nucl-th].

[6] F. M. Marqués and J. Carbonell, The quest for light multineutron systems, *Eur. Phys. J. A* **57**, 105 (2021), arXiv:2102.10879 [nucl-ex].

[7] F. M. Marqués, M. Labiche, A. Orr, N. A., *et al.*, Detection of neutron clusters, *Phys. Rev. C* **65**, 044006 (2002).

[8] K. Kisamori, S. Shimoura, H. Miya, *et al.*, Candidate resonant tetraneutron state populated by the ${}^4\text{He}({}^8\text{He}, {}^8\text{Be})$ reaction, *Phys. Rev. Lett.* **116**, 052501 (2016).

[9] T. Faestermann, A. Bergmaier, R. Gernhäuser, *et al.*, Indications for a bound tetraneutron, *Phys. Lett. B* **824**, 136799 (2022).

[10] R. Lazauskas, E. Hiyama, and J. Carbonell, Low energy structures in nuclear reactions with 4n in the finalstate, *Phys. Rev. Lett.* **130**, 102501 (2023), arXiv:2207.07575 [nucl-th].

[11] T. Faestermann and R. Gernhäuser, Recent results on the tetraneutron, arXiv preprint:2506.11623 (2025).

[12] P. Mueller, I. A. Sulai, A. C. C. Villari, *et al.*, Nuclear charge radius of ${}^8\text{He}$, *Phys. Rev. Lett.* **99**, 252501 (2007).

[13] G. Alkhazov, M. Andronenko, A. Dobrovolsky, *et al.*, Nuclear matter distributions in ${}^6\text{He}$ and ${}^8\text{He}$ from small angle p-He scattering in inverse kinematics at intermediate energy, *Phys. Rev. Lett.* **78**, 2313 (1997).

[14] U. van Kolck, Nucleon-nucleon interaction and isospin violation, *Lect. Notes Phys.* **513**, 62 (1998), arXiv:hep-ph/9711222.

[15] D. B. Kaplan, M. J. Savage, and M. B. Wise, A new expansion for nucleon-nucleon interactions, *Phys. Lett. B* **424**, 390 (1998), arXiv:nucl-th/9801034 [nucl-th].

[16] D. B. Kaplan, M. J. Savage, and M. B. Wise, Two nucleon systems from effective field theory, *Nucl. Phys. B* **534**, 329 (1998), arXiv:nucl-th/9802075 [nucl-th].

[17] U. van Kolck, Effective field theory of short range forces, *Nucl. Phys. A* **645**, 273 (1999), arXiv:nucl-th/9808007 [nucl-th].

[18] E. Braaten and H.-W. Hammer, Interpretation of neutral charm mesons near threshold as unparticles, *Phys. Rev. Lett.* **128**, 032002 (2022), arXiv:2107.02831 [hep-ph].

[19] E. Braaten and H.-W. Hammer, Point production of a nonrelativistic unparticle recoiling against a particle, *Phys. Rev. D* **107**, 034017 (2023), arXiv:2301.04399 [hep-th].

[20] S. Dietz, H.-W. Hammer, S. König, and A. Schwenk, Three-body resonances in pionless effective field theory, *Phys. Rev. C* **105**, 064002 (2022), arXiv:2109.11356 [nucl-th].

[21] E. Braaten and H. W. Hammer, Universality in few-body systems with large scattering length, *Phys. Rept.* **428**, 259 (2006), arXiv:cond-mat/0410417.

[22] W. Zwerger (editor), *The BCS-BEC crossover and the unitary Fermi gas* (Springer Berlin, Heidelberg, 2011).

[23] H. W. Hammer, C. Ji, and D. R. Phillips, Effective field theory description of halo nuclei, *J. Phys. G* **44**, 103002 (2017), arXiv:1702.08605 [nucl-th].

[24] H. W. Hammer, S. König, and U. van Kolck, Nuclear effective field theory: status and perspectives, *Rev. Mod. Phys.* **92**, 025004 (2020), arXiv:1906.12122 [nucl-th].

[25] M. D. Higgins, J. Golak, R. Skibiński, *et al.*, Observability of modified threshold behavior near unitarity: Md higgins et al., *Few-Body Systems* **66**, 35 (2025).

[26] F. Bringas, M. T. Yamashita, and T. Frederico, Triatomic continuum resonances for large negative scattering lengths, *Phys. Rev. A* **69**, 040702 (2004), arXiv:cond-mat/0312291.

[27] A. Deltuva, Energies and widths of Efimov states in the three-boson continuum, *Phys. Rev. C* **102**, 034003 (2020), arXiv:2101.12654.

[28] T. Hyodo, T. Hatsuda, and Y. Nishida, Universal physics of three bosons with isospin, *Phys. Rev. C* **89**, 032201 (2014), arXiv:1311.6289 [hep-ph].

[29] S. Jonsell, Efimov states for systems with negative scattering lengths, *Europhys. Lett.* **76**, 8 (2006).

[30] V. Efimov, Energy levels arising form the resonant two-body forces in a three-body system, *Phys. Lett. B* **33**, 563 (1970).

[31] L. Platter, H.-W. Hammer, and U.-G. Meißner, The four boson system with short range interactions, *Phys. Rev. A* **70**, 052101 (2004), arXiv:cond-mat/0404313.

[32] L. Platter, H.-W. Hammer, and U.-G. Meißner, On the correlation between the binding energies of the triton and the alpha-particle, *Phys. Lett. B* **607**, 254 (2005), arXiv:nucl-th/0409040.

[33] P. F. Bedaque and U. van Kolck, Nucleon deuteron scattering from an effective field theory, *Phys. Lett. B* **428**, 221 (1998), arXiv:nucl-th/9710073.

[34] P. F. Bedaque, H.-W. Hammer, and U. van Kolck, Effective theory for neutron deuteron scattering: energy dependence, *Phys. Rev. C* **58**, R641 (1998), arXiv:nucl-th/9802057.

[35] P. F. Bedaque, H.-W. Hammer, and U. van Kolck, Renormalization of the three-body system with short range interactions, *Phys. Rev. Lett.* **82**, 463 (1999), arXiv:nucl-th/9809025.

[36] P. F. Bedaque, H.-W. Hammer, and U. van Kolck, The three boson system with short range interactions, *Nucl. Phys. A* **646**, 444 (1999), arXiv:nucl-th/9811046.

[37] A. Gärdestig, Extracting the neutron-neutron scattering length—recent developments, *J. Phys. G* **36**, 053001 (2009), arXiv:0904.2787 [nucl-th].

[38] V. Babenko and N. Petrov, Study of the low-energy characteristics of neutron-neutron scattering in the effective-range approximation, arXiv preprint:1605.04849 (2016).

[39] R. Malone, A. Crowell, L. Cumberbatch, *et al.*, Measurement of the ${}^1\text{S}_0$ neutron-neutron effective range in neutron-deuteron breakup, *Phys. Lett. B* **835**, 137557 (2022).

[40] H.-W. Hammer and T. Mehen, A renormalized equation for the three-body system with short range interactions, *Nucl. Phys. A* **690**, 535 (2001), arXiv:nucl-th/0011024.

[41] Y. Nishida and D. T. Son, Nonrelativistic conformal field theories, *Phys. Rev. D* **76**, 086004 (2007), arXiv:0706.3746 [hep-th].

[42] Y. Nishida and D. T. Son, Unitary Fermi gas, epsilon expansion, and nonrelativistic conformal field theories, *Lect. Notes Phys.* **836**, 233 (2012), arXiv:1004.3597 [cond-mat.quant-gas].

[43] S. Ishikawa, Three-neutron bound and continuum states, *Phys. Rev. C* **102**, 034002 (2020).

[44] M. D. Higgins, C. H. Greene, A. Kievsky, and M. Viviani, Comprehensive study of the three- and four-neutron sys-

tems at low energies, Phys. Rev. C **103**, 024004 (2021).

[45] A. Deltuva, Three-neutron resonance study using transition operators, Phys. Rev. C **97**, 034001 (2018).

[46] P. F. Bedaque and U. Van Kolck, Nucleon-deuteron scattering from an effective field theory, Phys. Lett. B **428**, 221 (1998).

[47] S. D. Chowdhury, R. Mishra, and D. T. Son, Applied nonrelativistic conformal field theory: scattering-length and effective-range corrections to rate of production of three neutrons at low relative momenta, Phys. Rev. D **109**, 016001 (2024).

[48] K. Miki, K. Kameya, D. Sakai, *et al.*, Precise spectroscopy of the $3n$ and $3p$ systems via the ${}^3\text{H}(t, {}^3\text{He})3n$ and ${}^3\text{He}({}^3\text{He}, t)3p$ reactions at intermediate energies, Phys. Rev. Lett. **133**, 012501 (2024).

[49] L. Wu, S. Elhatisari, U.-G. Meißner, *et al.*, Search-
ing for the tetraneutron resonance on the lattice, arXiv:2601.01801 [nucl-th].

[50] S. Zhang, S. Elhatisari, and U.-G. Meißner, Multi-neutron correlations in light nuclei via ab-initio lattice simulations, arXiv:2512.18849 [nucl-th].

[51] E. P. Wigner, Lower limit for the energy derivative of the scattering phase shift, Phys. Rev. **98**, 145 (1955).

[52] D. R. Phillips and T. D. Cohen, How short is too short? Constraining contact interactions in nucleon-nucleon scattering, Phys. Lett. B **390**, 7 (1997), arXiv:nucl-th/9607048.

[53] H. W. Hammer and D. Lee, Causality and universality in low-energy quantum scattering, Phys. Lett. B **681**, 500 (2009), arXiv:0907.1763 [nucl-th].